Origin of the Tetragonal Ground State of Heusler Compounds

Sergey V. Faleev, Yari Ferrante, Jaewoo Jeong, Mahesh G. Samant, Barbara Jones, and Stuart S. P. Parkin

Phys. Rev. Applied **7**, 034022 — Published 24 March 2017

DOI: 10.1103/PhysRevApplied.7.034022

Origin of tetragonal ground state of Heusler compounds

Sergey V. Faleev,[1,*] Yari Ferrante,[1,2,3] Jaewoo Jeong,[1] Mahesh G. Samant,[1] Barbara Jones,[1] and Stuart S. P. Parkin[1,3,†]

[1]*IBM Research - Almaden, 650 Harry Road, San Jose, California 95120, USA*
[2]*Martin Luther University, 06099 Halle (Saale), Germany*
[3]*Max Planck Institute for Microstructure Physics, 06120 Halle (Saale), Germany*

(Dated: January 17, 2017)

In the present work we describe the general mechanism of tetragonal distortion in Heusler compounds X_2YZ. From 286 compounds studied using density functional theory (DFT) 62% were found to be tetragonal at zero temperature. Such a large share of compounds with tetragonal distortions can be explained by the peak-and-valley character of density of states (DOS) of these compounds in cubic phase (arising from localized *d*-bands and van Hove singularities) in conjunction with a smooth shift of peaky DOS structure relative to the Fermi energy, E_F, when valence electrons are added to the system. A shift of DOS in Y or Z-series leads to alternation of stable and nonstable cubic phases depending on the value of DOS at E_F in the cubic phase. Groups of compounds with a large share of tetragonal distortions are identified and explained.

PACS numbers: 73.40.Rw, 85.75.-d

I. INTRODUCTION

Key to the successful development of spin-transfer torque magnetic random access memory (STT-MRAM), one of the most promising emerging non-volatile memory technologies today, are new magnetic materials for magnetic tunnel junction (MTJ) memory elements that have sufficient stability against thermal fluctuations to sustain deeply scaled devices. These materials must possess sufficient perpendicular magnetic anisotropy (PMA) that their magnetizations lie perpendicular to the plane of the MTJ device, since this allows for reduced currents to switch the magnetization of the electrode using spin torque [1, 2]. The most promising magnetic materials to date are considered to be alloys of Co, Fe and B, in conjunction with MgO tunnel barriers [1, 3, 4]. Unfortunately, PMA of CoFeB layers arises from the interfaces between these layers and the tunnel barrier and/or the underlayer and is too weak to overcome thermal fluctuations when the device has a critical dimension $\lesssim$ 20nm.

Magnetic materials in which the PMA is derived from volume magnetocrystalline anisotropy are needed. One of the most promising class of such materials are the Heusler compounds X_2YZ wherein X and Y are transition metals, or lanthanides, and Z is the main group element [5]. While many Heuslers are cubic (so PMA is zero), some of these compounds are found to be tetragonally distorted and thus could potentially have large PMA.

Some examples of tetragonal Heusler compounds are $Mn_{3-x}Ga$ [6] and Mn_3Ge [7]. Thin films of these materials have been shown to exhibit large PMA for films grown epitaxially on single crystalline substrates such as SrTiO3(001) or MgO(001) [7–11] and on amorphous substrates ($Si(001)/SiO_2$) [12]. Unfortunately, the experimental values of the tunneling magnetoresistance (TMR) for MTJs with $Mn_{3-x}Ga$ or Mn_3Ge electrodes and MgO tunnel barriers is found to be very small, far below those needed for applications [12]. Whilst the reason for the low values of TMR is not fully understood in these materials, the identification of other tetragonal Heusler compounds that may potentially have high PMA with high TMR is important.

Despite potential importance of tetragonal Heusler compounds for spintronic applications there is still a lack of fundamental understanding of which Heuslers display a tetragonal ground state. To date most of the known tetragonal Heuslers are Mn-based. Tetragonal distortion in Mn-based compounds is usually explained by the susceptibility of the octahedrally-coordinated Mn atom to a band Jahn-Teller distortion [5, 13]. Such explanation, though, cannot be applied to non Mn-based Heuslers and even for Mn-based is not universal [14].

In this paper we give a general explanation of the origin of the tetragonal distortion in Heuslers based on systematic study of 286 compounds. We explain why some groups of compounds are more susceptible to a distortion thus providing a guidance for experimental and theoretical efforts in finding tetragonal Heuslers with high PMA.

II. CRYSTAL STRUCTURE

Cubic Heusler compounds X_2YZ can have *regular* structure or *inverse* structure. These two crystal structures are shown in Fig. 1(a) and (c) with four sites forming four fcc sublattices: site Z (occupied by atom Z), site II, octahedrally coordinated by Z, and two equivalent sites I tetrahedrally coordinated by Z. In regular structure shown on Fig 1(a) two X atoms [red, labeled as X(I)] have identical environment - they are located on sites I in the same *xy*-plane. In this structure the Y atom

*Electronic address: svfaleev@us.ibm.com
†Electronic address: stuart.parkin@mpi-halle.mpg.de

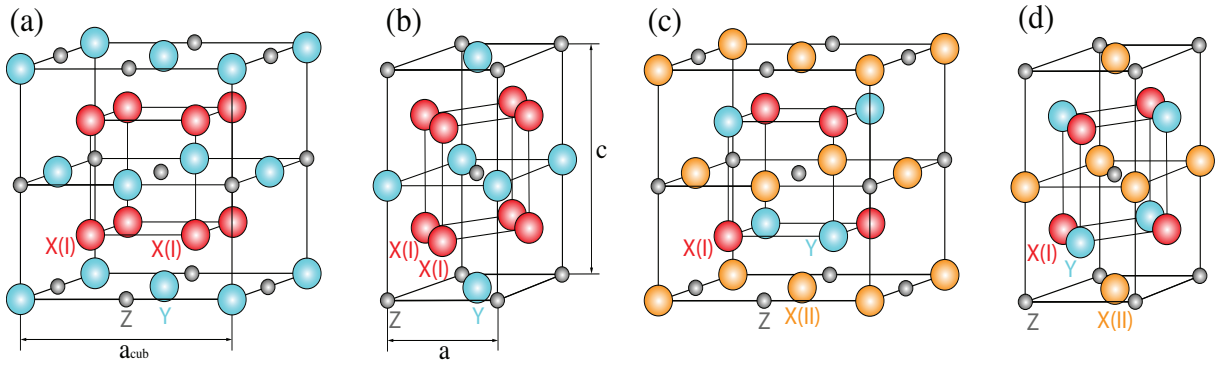

FIG. 1: (a) regular and (c) inverse cubic Heusler structure. (b) regular and (d) inverse tetragonal Heusler structure.

(cyan) on site II and Z atom (grey) are located in another xy-plane. In inverse structure shown on Fig 1(c) two X atoms have different environment - one X atom [red, labeled as X(I)] is located on site I in one xy-plane with Y atom (cyan), while another X atom [orange, labeled as X(II)] is located on site II in one xy-plane with Z atom (grey).

Regular [Fig 1(b)] and inverse [Fig 1(d)] tetragonal Heusler structures can be obtained from regular and inverse cubic structures, correspondingly, by stretching (or compressing) parent cubic structure along the z-axis. Tetragonal unit cells shown on Fig 1(b) and Fig 1(d) are rotated on 45^o around z-axis relative to the parent cubic structures shown on Fig 1(a) and Fig 1(c), correspondingly. (Note that only part of atoms from Fig 1(a) and Fig 1(c) are shown on Fig 1(b) and Fig 1(d).) Lattice constant a_{cub} of the cubic Heusler is shown on Fig 1(a) and lattice constants a and c of the tetragonal Heusler are shown on Fig 1(b). For characterization of the tetragonal unit cell we use dimensionless parameter $c' = c/(2a)$ that is equal to $1/\sqrt{2}$ for the cubic structure, and vary between 0.8 and 1.1 for most of the tetragonal Heuslers we found (see Tables I and II). Note that for $c' = 1$ tetragonal structure would become the *fcc* structure if all four atoms of the compound could be considered as equivalent.

III. LATTICE PARAMETERS AND ENERGY STABILITY OF 286 HEUSLER COMPOUNDS

We performed DFT calculations for both the regular and inverse structures and various magnetic configurations for 286 Hesler compounds using the VASP program [15] with PAW potentials and PBE GGA/DFT functional [16, 17]. Calculated lattice parameters a and c' for Heusler compounds X_2YZ with X={Mn,Fe,Co} and YZ= {Mn,Fe,Co,Ni,Cu}{Al,Ga,Si,Ge,Sn,Sb}, and YZ={Mo,Ru,Rh,Pd,W,Os,Ir,Pt}{Ga,In,Ge,Sn,Sb} are shown in Table I. Calculated lattice parameters a and c' for ternary Heusler compounds X_2YZ with X={Ru,Rh,Pd} and YZ={Mn,Fe,Co}{Ga,In,Ge,Sn,Sb}, X=Ni and YZ={Mn,Fe,Co}{Al,Ga,Si,Ge,Sn,Sb}, X=Mn and YZ= {Fe,Co,Ni,Cu}{In}, and binary compounds X_3Z with X={Mn,Fe,Co} and Z={In,P,As} are shown in Table II.

For ternary compounds symbol s_1 in Tables I and II labels the minimal energy configuration as follows: $s_1 = tr, ti, cr$, or ci represent tetragonal regular, tetragonal inverse, cubic regular, or cubic inverse minimal energy configuration, correspondingly. For the case of binary compound X_3Z symbol $s_1 = t$ or c represent tetragonal or cubic minimal energy configuration, correspondingly. If minimal energy configuration is tetragonal then tetragonal lattice parameters a_t and c'_t are shown together with corresponding cubic lattice constant a_c that corresponds to the local minimum of the total energy with fixed $c' = 1/\sqrt{2}$ and the same chemical ordering (regular or inverse) and initial (in the input of the VASP program) configuration of magnetic moments as tetragonal configuration. Conventional cubic lattice constant a_{cub} shown on Fig 1(a) could be obtained from a_c as $a_{cub} = \sqrt{2}a_c$. We presented the a_c values in the Tables I and II instead of conventional a_{cub} since it is the a_c (and a_t) lattice constant of the Heusler compound that, ideally, should match the lattice constant of MgO ($a_{MgO} = 4.21$ Å) which is conventional spacer used in most of the MTJ devices.

The m_t and m_c are the magnetic moments (per formula unit) of the tetragonal and cubic phases, correspondingly. The m_c values that satisfy the Slater-Pauling rule within $\pm 0.5\mu_B$ tolerance are indicated by green color in Tables I and II. Slater-Pauling rule describes relationship between magnetic moment, M (in μ_B), of Heusler compound per formula unit and the number of the valence electrons, N_V per formula unit [5, 18, 19]:

$$M = N_V - 24\ . \qquad (1)$$

For the sign of the spin direction we adopted convention that in the case of the ferrimagnetic coupling of the $X(I)$ atom with $X(II)$ atom or Y atom, or both, the sign of the magnetic moment of the $X(I)$ atom is assumed to be negative. Such convention makes the analysis of the density of states (DOS) figures presented in this paper more convenient since DOS of electrons with positive and negative spin directions (that we will continue to call

TABLE I: Calculated lattice parameters a_t, c_t' and magnetic moment m_t of tetragonal phase, lattice constant a_c and magnetic moment m_c of cubic phase, and total energy differences E_{ct} and E_{21} for Heusler compounds X_2YZ with X={Mn,Fe,Co} and YZ={Mn,Fe,Co,Ni,Cu}{Al,Ga,Si,Ge,Sn,Sb}, and YZ={Mo,Ru,Rh,Pd,W,Os,Ir,Pt} {Ga,In,Ge,Sn,Sb}. The m_c values that satisfy the Slater-Pauling rule, Eq. (1), within $\pm 0.5\mu_B$ tolerance are indicated by green color. Symbols s_1 and s_2 label the lowest and second lowest energy configuration (see text for details).

	s_1	a_t (Å)	c_t'	m_t (μ_B)	a_c (Å)	m_c (μ_B)	E_{ct} (eV)	s_2	E_{21} (eV)
Mn_3Al	t	3.81	0.91	-1.67	4.09	0.00	0.04	t	0.32
Mn_2FeAl	ti	3.69	0.98	-0.85	4.06	1.00	0.01	tr	0.23
Mn_2CoAl	ci				4.06	2.00		tr	0.37
Mn_2NiAl	ti	3.81	0.88	1.01	4.11	1.15	0.06	tr	0.29
Mn_2CuAl	ci				4.16	0.15		tr	0.24
Mn_3Ga	t	3.78	0.94	-1.79	4.12	0.00	0.19	t	0.35
Mn_2FeGa	ti	3.69	0.98	-0.84	4.09	1.02	0.14	tr	0.25
Mn_2CoGa	ci	3.71	0.96	0.14	4.08	2.00	-0.03	tr	0.26
Mn_2NiGa	ti	3.79	0.90	0.99	4.13	1.16	0.12	tr	0.16
Mn_2CuGa	ci				4.20	0.30		tr	0.10
Mn_3Si	c	3.66	0.95	-0.98	3.99	1.00	-0.09	t	0.44
Mn_2FeSi	ci	3.59	0.98	-0.11	3.96	2.00	-0.27	cr	0.41
Mn_2CoSi	ci	3.69	0.90	1.03	3.97	3.00	-0.08	tr	0.35
Mn_2NiSi	ti	3.61	0.97	0.32	4.02	1.07	0.10	tr	0.16
Mn_2CuSi	tr	3.71	0.94	4.92	4.06	4.43	0.21	ci	0.19
Mn_3Ge	t	3.73	0.95	-1.01	4.06	1.00	0.10	t	0.58
Mn_2FeGe	ci	3.62	1.03	-0.86	4.05	2.00	-0.06	tr	0.33
Mn_2CoGe	ti	3.74	0.92	0.97	4.06	3.00	0.07	tr	0.29
Mn_2NiGe	ti	3.73	0.95	0.31	4.13	0.88	0.08	tr	0.09
Mn_2CuGe	tr	3.77	0.95	5.28	4.15	4.64	0.32	ci	0.21
Mn_3Sn	t	3.93	0.95	-1.04	4.27	1.00	0.34	t	0.48
Mn_2FeSn	ti	3.83	1.01	-0.90	4.27	2.00	0.04	tr	0.17
Mn_2CoSn	ti	3.96	0.90	1.00	4.30	1.49	0.15	tr	0.25
Mn_2NiSn	ti	4.09	0.85	0.34	4.35	0.52	0.01	tr	0.16
Mn_2CuSn	tr	3.91	0.98	5.73	4.42	6.64	0.32	ci	0.06
Mn_3Sb	t	3.82	1.02	-1.14	4.23	2.00	0.18	t	0.42
Mn_2FeSb	ci	3.93	0.91	0.97	4.23	3.00	0.00	tr	0.11
Mn_2CoSb	ci				4.23	4.00		ti	0.04
Mn_2NiSb	tr	3.81	1.02	5.85	4.33	6.32	0.61	ti	0.11
Mn_2CuSb	tr	3.86	1.01	5.45	4.42	6.48	0.45	ti	0.27
Mn_2MoGa	cr				4.17	-1.00		cr	0.05
Mn_2RuGa	ti	3.81	0.97	-0.26	4.21	1.02	0.10	tr	0.25
Mn_2RhGa	ti	3.83	0.97	0.07	4.23	1.68	0.17	tr	0.30
Mn_2PdGa	ti	3.93	0.92	0.92	4.33	0.55	0.10	tr	0.12
Mn_2MoIn	tr	4.09	0.88	-3.73	4.33	-1.01	0.09	cr	0.16
Mn_2RuIn	ti	3.94	1.00	-0.30	4.41	1.02	0.24	tr	0.21
Mn_2RhIn	ti	3.98	0.98	0.05	4.44	0.88	0.22	tr	0.23
Mn_2PdIn	ti	4.18	0.88	0.30	4.50	0.38	0.03	tr	0.07
Mn_2MoGe	cr				4.15	0.00		ti	0.15
Mn_2RuGe	ti	3.81	0.96	0.00	4.17	2.00	0.00	tr	0.53
Mn_2RhGe	ti	3.85	0.94	0.77	4.18	3.00	0.22	tr	0.29
Mn_2PdGe	ti	3.91	0.95	0.09	4.33	0.57	0.10	tr	0.03
Mn_2MoSn	ti	3.86	1.08	0.14	4.45	0.04	0.26	cr	0.07
Mn_2RuSn	ti	3.97	0.97	0.00	4.38	1.73	0.21	tr	0.43
Mn_2RhSn	ti	4.03	0.93	0.75	4.44	0.52	0.14	tr	0.25
Mn_2PdSn	ti	4.17	0.89	0.20	4.50	0.43	0.05	tr	0.10
Mn_2MoSb	ti	3.88	1.06	-0.20	4.41	1.00	0.26	ti	0.33
Mn_2RuSb	ti	3.94	0.98	0.17	4.33	3.00	0.17	tr	0.40
Mn_2RhSb	ti	4.00	0.96	0.00	4.44	0.51	0.17	tr	0.16
Mn_2PdSb	tr	4.04	0.99	7.20	4.54	7.47	0.30	ci	0.02
Mn_2WGa	cr				4.18	-0.95		cr	0.03
Mn_2OsGa	ti	3.80	0.98	-0.28	4.21	1.00	0.15	tr	0.34
Mn_2IrGa	ti	3.83	0.97	0.07	4.21	2.00	0.27	tr	0.40
Mn_2PtGa	ti	3.90	0.94	0.87	4.33	0.47	0.18	tr	0.11
Mn_2WIn	cr				4.33	-0.96		cr	0.05
Mn_2OsIn	ti	3.92	1.01	-0.29	4.42	0.68	0.36	tr	0.27
Mn_2IrIn	ti	3.96	0.99	0.04	4.45	0.71	0.31	tr	0.30
Mn_2PtIn	ti	4.11	0.92	0.44	4.51	0.32	0.08	tr	0.02
Mn_2WGe	cr				4.16	0.00		ti	0.43
Mn_2OsGe	ti	3.81	0.97	-0.03	4.18	2.00	0.06	tr	0.51
Mn_2IrGe	ti	3.83	0.96	0.51	4.19	3.00	0.28	tr	0.25
Mn_2PtGe	tr	4.88	0.97	0.00	4.36	0.00	0.35	ti	0.11
Mn_2WSn	cr				4.31	0.00		ti	0.40
Mn_2OsSn	ti	3.96	0.98	-0.02	4.37	2.00	0.33	tr	0.50
Mn_2IrSn	ti	3.99	0.96	0.46	4.45	0.44	0.22	tr	0.22
Mn_2PtSn	tr	4.05	0.96	0.00	4.50	0.00	0.28	ti	0.05
Mn_2WSb	ti	3.84	1.08	-0.06	4.41	1.00	0.47	cr	0.23
Mn_2OsSb	ti	3.96	0.97	0.17	4.35	3.00	0.24	tr	0.32
Mn_2IrSb	ti	3.96	0.99	-0.21	4.47	0.04	0.18	tr	0.02
Mn_2PtSb	tr	4.10	0.94	0.00	4.52	0.00	0.14	tr	0.01
Fe_2MnAl	cr				4.01	2.00		ti	0.25
Fe_3Al	c				4.06	5.94		t	0.70
Fe_2CoAl	ci				4.03	4.96		tr	0.32
Fe_2NiAl	ci				4.06	4.78		tr	0.07
Fe_2CuAl	tr	3.57	1.08	4.65	4.10	3.99	0.56	ci	0.16
Fe_2MnGa	cr				4.02	2.02		ti	0.03
Fe_3Ga	t	3.83	0.86	6.62	4.07	6.05	0.02	t	0.65
Fe_2CoGa	ci				4.05	5.11		tr	0.17
Fe_2NiGa	ci				4.07	4.86		tr	0.03
Fe_2CuGa	tr	3.60	1.06	4.73	4.13	4.45	0.52	ti	0.22
Fe_2MnSi	cr				3.95	3.00		ci	0.27
Fe_3Si	c				3.96	5.01		t	0.68
Fe_2CoSi	ci				3.96	4.93		tr	0.38
Fe_2NiSi	tr	3.49	1.06	4.68	3.95	3.18	0.40	ci	0.12
Fe_2CuSi	tr	3.55	1.03	4.24	3.98	2.50	0.11	ti	0.10
Fe_2MnGe	cr				4.02	3.00		ti	0.17
Fe_3Ge	c				4.04	5.24		t	0.62
Fe_2CoGe	ci				4.04	5.05		tr	0.28
Fe_2NiGe	tr	3.54	1.07	4.83	4.05	3.89	0.51	ci	0.16
Fe_2CuGe	tr	3.61	1.05	4.59	4.08	3.55	0.29	ti	0.15
Fe_2MnSn	ti	3.97	0.90	7.34	4.31	7.57	0.08	cr	0.15
Fe_3Sn	c				4.25	6.46		t	0.76
Fe_2CoSn	ci				4.23	5.41		tr	0.26
Fe_2NiSn	tr	3.68	1.09	4.97	4.25	4.63	0.62	ci	0.06
Fe_2CuSn	tr	3.76	1.06	4.87	4.30	4.36	0.43	ti	0.11
Fe_2MnSb	cr				4.20	4.05		ti	0.16
Fe_3Sb	c				4.23	6.06		t	0.71
Fe_2CoSb	ci				4.23	5.87		tr	0.19
Fe_2NiSb	tr	3.70	1.09	5.41	4.22	4.16	0.45	ti	0.13
Fe_2CuSb	tr	3.79	1.05	5.06	4.27	3.86	0.23	ti	0.02
Fe_2MoGa	tr	4.06	0.75	0.88	4.14	0.87	0.01	tr	0.04
Fe_2RuGa	ci				4.19	5.47		tr	0.35
Fe_2RhGa	ci				4.18	5.04		tr	0.33
Fe_2PdGa	ci	3.88	0.91	4.91	4.22	4.94	-0.01	tr	0.07
Fe_2MoIn	cr				4.30	1.00		ti	0.16
Fe_2RuIn	ci				4.36	5.81		tr	0.21
Fe_2RhIn	ci				4.36	5.34		tr	0.26
Fe_2PdIn	ti	4.01	0.93	5.11	4.40	5.20	0.01	tr	0.10
Fe_2MoGe	tr	3.85	0.88	0.00	4.15	1.85	0.06	ci	0.05
Fe_2RuGe	ci				4.16	4.97		ti	0.48
Fe_2RhGe	ci				4.18	4.98		tr	0.38
Fe_2PdGe	tr	3.67	1.09	5.12	4.23	4.65	0.52	ti	0.07
Fe_2MoSn	cr				4.31	2.12		ti	0.12
Fe_2RuSn	ci				4.34	5.21		tr	0.52
Fe_2RhSn	ci				4.35	5.15		tr	0.35
Fe_2PdSn	tr	3.82	1.08	5.16	4.39	4.84	0.50	ci	0.02
Fe_2MoSb	ti	3.78	1.08	1.34	4.38	4.15	0.12	cr	0.08
Fe_2RuSb	ci				4.33	4.95		ti	0.52
Fe_2RhSb	ci				4.35	5.50		tr	0.12
Fe_2PdSb	tr	3.86	1.06	5.57	4.38	4.63	0.36	ti	0.10
Fe_2WGa	cr				4.15	0.94		tr	0.04
Fe_2OsGa	ci				4.20	5.12		ti	0.10
Fe_2IrGa	ci				4.20	5.13		tr	0.41
Fe_2PtGa	ti	3.88	0.92	5.05	4.24	5.13	0.02	tr	0.11
Fe_2WIn	cr				4.30	1.03		tr	0.04
Fe_2OsIn	ti	3.89	1.00	5.74	4.37	5.78	0.03	ti	0.05
Fe_2IrIn	ci				4.38	5.56		tr	0.25
Fe_2PtIn	ti	3.97	0.96	5.24	4.40	5.34	0.07	tr	0.15
Fe_2WGe	tr	3.85	0.88	0.00	4.16	1.90	0.04	ti	0.22
Fe_2OsGe	ci				4.19	4.99		ti	0.31
Fe_2IrGe	ci				4.19	4.97		tr	0.40
Fe_2PtGe	tr	3.68	1.10	5.25	4.25	4.53	0.60	ti	0.10
Fe_2WSn	cr				4.31	1.99		tr	0.19
Fe_2OsSn	ci				4.36	5.28		ti	0.32
Fe_2IrSn	ci				4.37	5.21		tr	0.32
Fe_2PtSn	tr	3.85	1.06	5.17	4.39	4.75	0.51	ti	0.03
Fe_2WSb	cr				4.32	2.80		ti	0.11
Fe_2OsSb	ci				4.35	5.00		ti	0.37
Fe_2IrSb	ti	3.92	0.97	5.07	4.38	5.59	0.03	tr	0.07
Fe_2PtSb	tr	3.87	1.06	5.61	4.37	4.33	0.40	ti	0.17
Co_2MnAl	cr				4.03	4.01		ti	0.71
Co_2FeAl	cr				4.03	4.98		ti	0.61
Co_3Al	c	3.70	0.90	3.63	4.01	3.98	-0.07	t	0.24
Co_3NiAl	ti	3.67	0.92	2.65	4.02	2.97	0.15	tr	0.13
Co_3CuAl	ti	3.71	0.92	2.45	4.06	2.56	0.03	cr	0.05
Co_2MnGa	cr				4.05	4.08		ti	0.59
Co_2FeGa	cr				4.05	5.00		ti	0.51
Co_3Ga	c	3.66	0.94	3.74	4.03	4.06	-0.01	t	0.23
Co_2NiGa	ti	3.69	0.92	2.73	4.03	2.99	0.18	tr	0.10
Co_2CuGa	ti	3.70	0.94	2.58	4.07	2.63	0.06	cr	0.05
Co_2MnSi	cr				3.98	5.00		ti	0.65
Co_2FeSi	cr				3.98	5.46		ti	0.33
Co_3Si	t	3.58	0.93	2.79	3.95	3.80	0.15	t	0.12
Co_2NiSi	ti	3.55	0.96	2.23	3.95	2.38	0.31	tr	0.05
Co_2CuSi	cr				3.94	0.00		ti	0.56
Co_2MnGe	cr				4.06	5.00		ti	0.62
Co_2FeGe	cr				4.06	5.63		ti	0.32
Co_3Ge	t	3.64	0.94	2.99	4.03	3.95	0.13	t	0.18
Co_2NiGe	ti	3.62	0.96	2.37	4.05	2.58	0.30	tr	0.02
Co_2CuGe	cr				4.02	0.01		ti	0.43
Co_2MnSn	cr				4.23	5.01		ti	0.67
Co_2FeSn	cr				4.24	5.70		ti	0.41
Co_3Sn	t	3.81	0.94	3.17	4.21	4.00	0.08	t	0.28
Co_2NiSn	ti	3.80	0.95	2.49	4.21	2.63	0.22	tr	0.09
Co_2CuSn	cr				4.20	0.17		ti	0.28
Co_2MnSb	cr				4.25	6.00		ti	0.54
Co_2FeSb	tr	3.97	0.85	4.81	4.22	5.35	0.14	ti	0.19
Co_3Sb	t	3.77	0.95	2.49	4.20	3.92	0.28	t	0.22
Co_2NiSb	tr	3.81	0.92	1.27	4.18	1.84	0.14	ti	0.02
Co_2CuSb	tr	3.99	0.82	0.00	4.19	0.63	0.03	ti	0.46
Co_2MoGa	tr	3.80	0.92	0.79	4.17	2.89	0.12	ti	0.27
Co_2RuGa	ci	3.68	0.98	0.24	4.14	3.80	-0.07	tr	0.04
Co_2RhGa	ti	3.81	0.91	3.29	4.14	3.34	0.02	tr	0.15
Co_2PdGa	ti	3.82	0.92	2.78	4.18	3.03	0.22	tr	0.18
Co_2MoIn	cr				4.33	2.99		ti	0.49
Co_2RuIn	ci				4.31	4.52		ti	0.17
Co_2RhIn	ti	3.89	0.96	3.47	4.32	3.51	0.10	tr	0.13
Co_2PdIn	ti	3.93	0.95	2.96	4.35	3.13	0.20	tr	0.16
Co_2MoGe	tr	3.72	0.98	0.15	4.18	3.51	0.42	ti	0.04
Co_2RuGe	ci	3.73	0.94	0.13	4.13	3.19	-0.04	tr	0.13
Co_2RhGe	ti	3.78	0.92	2.69	4.15	3.34	0.23	tr	0.27
Co_2PdGe	ti	3.76	0.96	2.49	4.18	2.75	0.36	tr	0.17
Co_2MoSn	tr	4.07	0.84	2.12	4.33	3.94	0.07	ti	0.27
Co_2RuSn	ti	3.88	0.96	3.14	4.30	3.32	0.01	tr	0.09
Co_2RhSn	ti	3.92	0.93	2.87	4.32	3.38	0.23	tr	0.23
Co_2PdSn	ti	3.89	0.97	2.54	4.36	2.87	0.29	tr	0.15
Co_2MoSb	ti	3.77	1.06	1.30	4.32	0.00	0.31	tr	0.01
Co_2RuSb	ti	3.87	0.95	2.43	4.30	3.21	0.17	tr	0.27
Co_2RhSb	ti	3.88	0.95	2.34	4.31	3.26	0.46	tr	0.25
Co_2PdSb	ti	3.88	0.98	2.75	4.35	2.71	0.35	tr	0.04
Co_2WGa	tr	3.88	0.87	1.07	4.16	1.72	0.13	ti	0.32
Co_2OsGa	tr	3.70	0.97	0.57	4.16	4.08	0.25	ti	0.06
Co_2IrGa	ti	3.77	0.95	3.09	4.16	3.40	0.05	tr	0.08
Co_2PtGa	ti	3.80	0.94	2.82	4.20	3.23	0.33	tr	0.18
Co_2WIn	tr	4.13	0.80	1.42	4.31	1.80	0.04	tr	0.11
Co_2OsIn	cr				4.31	4.44		ti	0.28
Co_2IrIn	ti	3.82	1.02	3.37	4.34	3.60	0.18	tr	0.11
Co_2PtIn	ti	3.90	0.98	3.01	4.38	3.34	0.34	tr	0.14
Co_2WGe	tr	3.74	0.97	0.00	4.16	0.73	0.41	ti	0.04
Co_2OsGe	ti	3.74	0.94	0.26	4.15	3.10	0.07	tr	0.03
Co_2IrGe	ti	3.76	0.95	2.51	4.17	3.24	0.24	tr	0.24
Co_2PtGe	ti	3.76	0.97	2.44	4.22	3.10	0.52	tr	0.16
Co_2WSn	tr	4.07	0.84	1.76	4.31	0.79	0.11	ti	0.30
Co_2OsSn	tr	3.87	0.95	0.20	4.31	3.79	0.24	ti	0.04
Co_2IrSn	ti	3.88	0.97	2.79	4.35	3.41	0.29	tr	0.20
Co_2PtSn	ti	3.89	0.98	2.52	4.38	3.10	0.49	tr	0.11
Co_2WSb	ti	3.76	1.07	1.12	4.33	0.00	0.48	tr	0.05
Co_2OsSb	ti	3.86	0.97	2.19	4.31	2.95	0.23	tr	0.23
Co_2IrSb	ti	3.86	0.97	2.34	4.33	3.34	0.51	tr	0.27
Co_2PtSb	ti	3.86	1.00	2.63	4.38	2.87	0.59	tr	0.03

TABLE II: Same as Table I for ternary Heusler compounds X_2YZ with X={Ru,Rh,Pd} and YZ={Mn,Fe,Co}{Ga,In,Ge,Sn,Sb}, X=Ni and YZ={Mn,Fe,Co}{Al,Ga,Si,Ge,Sn,Sb}, X=Mn and YZ={Fe,Co,Ni,Cu}{In}, and binary compounds X_3Z with X={Mn,Fe,Co} and Z={In,P,As}. (Note that binary compounds X_3Z with X={Mn,Fe,Co} and Z={Al,Ga,Si,Ge,Sn,Sb} are shown in Table I.)

	s_1	a_t (Å)	c'_t	m_t (μ_B)	a_c (Å)	m_c (μ_B)	E_{ct} (eV)	s_2	E_{21} (eV)
Ru_2MnGa	cr				4.23	2.13		ti	0.66
Ru_2FeGa	cr				4.24	3.14		ti	0.45
Ru_2CoGa	ti	3.72	1.02	1.06	4.24	2.74	0.42	cr	0.11
Ru_2MnIn	cr				4.40	2.19		ti	0.39
Ru_2FeIn	cr				4.40	3.25		ti	0.25
Ru_2CoIn	ti	3.89	0.99	1.28	4.40	3.68	0.27	cr	0.22
Ru_2MnGe	cr				4.25	3.03		ti	0.80
Ru_2FeGe	cr				4.24	3.96		ti	0.66
Ru_2CoGe	cr				4.21	1.96		ti	0.13
Ru_2MnSn	cr				4.41	3.07		ti	0.65
Ru_2FeSn	cr				4.40	4.13		ti	0.64
Ru_2CoSn	ti	3.90	0.98	0.04	4.40	3.69	0.47	cr	0.07
Ru_2MnSb	cr				4.41	4.01		ti	0.83
Ru_2FeSb	cr				4.40	4.37		ti	0.65
Ru_2CoSb	cr				4.37	2.82		ti	0.15
Ni_2MnAl	cr				4.09	4.02		ti	0.27
Ni_2FeAl	tr	3.68	0.94	3.20	4.06	3.17	0.04	ti	0.09
Ni_2CoAl	tr	3.61	0.97	1.93	4.02	1.55	0.24	ti	0.04
Ni_2MnGa	tr	3.80	0.89	4.00	4.10	4.01	0.03	ti	0.18
Ni_2FeGa	tr	3.67	0.96	3.30	4.08	3.23	0.07	ti	0.12
Ni_2CoGa	tr	3.61	0.98	2.03	4.04	1.67	0.25	ti	0.02
Mn_3In	t	3.95	0.96	-1.93	4.44	-2.60	0.26	t	0.57
Mn_2FeIn	ti	3.89	0.98	-0.94	4.33	1.26	0.19	ti	0.18
Mn_2CoIn	ti	3.90	0.96	0.08	4.31	1.87	0.06	tr	0.20
Mn_2NiIn	ti	4.02	0.89	0.86	4.35	0.54	0.01	tr	0.11
Mn_2CuIn	ci				4.41	0.26		tr	0.19

	s_1	a_t (Å)	c'_t	m_t (μ_B)	a_c (Å)	m_c (μ_B)	E_{ct} (eV)	s_2	E_{21} (eV)
Rh_2MnGa	cr				4.28	4.09		ti	0.74
Rh_2FeGa	cr				4.27	4.27		ti	0.72
Rh_2CoGa	cr				4.24	3.00		ti	0.35
Rh_2MnIn	cr				4.44	4.29		ti	0.63
Rh_2FeIn	cr				4.42	4.24		ti	0.56
Rh_2CoIn	cr				4.40	3.01		ti	0.21
Rh_2MnGe	tr	4.16	0.78	4.35	4.29	4.73	0.01	ti	0.73
Rh_2FeGe	tr	4.01	0.85	3.83	4.28	3.54	0.21	ti	0.66
Rh_2CoGe	tr	3.95	0.87	2.22	4.25	2.33	0.19	ti	0.44
Rh_2MnSn	tr	4.32	0.77	4.45	4.45	4.76	0.01	ti	0.72
Rh_2FeSn	tr	4.16	0.85	3.89	4.42	3.54	0.19	ti	0.64
Rh_2CoSn	tr	4.07	0.88	2.30	4.40	2.34	0.21	ti	0.37
Rh_2MnSb	tr	4.15	0.86	4.17	4.45	4.67	0.20	ti	0.64
Rh_2FeSb	tr	4.05	0.91	3.38	4.44	3.18	0.37	ti	0.50
Rh_2CoSb	tr	4.01	0.92	2.05	4.38	1.61	0.48	ti	0.44
Ni_2MnSi	tr	3.85	0.81	3.74	4.03	3.80	0.01	ti	0.04
Ni_2FeSi	ti	3.58	0.96	2.62	3.97	2.53	0.05	tr	0.03
Ni_2CoSi	ti	3.60	0.92	0.89	3.95	0.00	0.11	tr	0.12
Ni_2MnGe	tr	3.91	0.82	3.88	4.11	3.93	0.01	ti	0.07
Ni_2FeGe	ti	3.64	0.98	2.94	4.06	2.81	0.06	tr	0.01
Ni_2CoGe	ti	3.66	0.93	1.03	4.03	0.45	0.13	tr	0.11
Fe_3In	t	3.98	0.88	7.11	4.28	7.03	0.05	t	0.59
Mn_3P	c	3.50	1.04	-0.96	3.92	2.00	-0.21	t	0.42
Fe_3P	c				3.92	4.99		t	0.31
Co_3P	t	3.50	0.97	2.33	3.93	3.98	0.40	t	0.16

	s_1	a_t (Å)	c'_t	m_t (μ_B)	a_c (Å)	m_c (μ_B)	E_{ct} (eV)	s_2	E_{21} (eV)
Pd_2MnGa	tr	4.02	0.91	4.09	4.38	4.08	0.04	ti	0.23
Pd_2FeGa	tr	3.96	0.93	3.22	4.35	3.13	0.09	ti	0.27
Pd_2CoGa	tr	3.92	0.93	1.94	4.30	1.67	0.21	ti	0.26
Pd_2MnIn	cr	4.16	0.91	4.16	4.54	4.19	-0.01	ti	0.22
Pd_2FeIn	tr	4.09	0.93	3.20	4.50	3.18	0.06	ti	0.23
Pd_2CoIn	tr	4.03	0.95	1.94	4.46	1.74	0.21	ti	0.23
Pd_2MnGe	cr				4.40	4.11		ti	0.14
Pd_2FeGe	tr	3.91	0.97	3.12	4.36	3.24	0.10	ti	0.15
Pd_2CoGe	tr	3.90	0.95	1.71	4.32	1.64	0.21	ti	0.11
Pd_2MnSn	cr				4.54	4.14		ti	0.26
Pd_2FeSn	tr	4.13	0.91	3.03	4.51	3.21	0.04	ti	0.17
Pd_2CoSn	tr	4.03	0.95	1.61	4.46	1.65	0.19	ti	0.10
Pd_2MnSb	tr	4.33	0.83	4.21	4.58	4.30	0.01	ti	0.17
Pd_2FeSb	tr	4.04	0.98	3.23	4.54	3.40	0.05	ti	0.04
Pd_2CoSb	ti	4.12	0.89	1.25	4.45	1.08	0.05	tr	0.10
Ni_2MnSn	cr				4.29	4.06		ti	0.32
Ni_2FeSn	cr				4.25	3.25		ti	0.14
Ni_2CoSn	ti	3.81	0.94	1.07	4.18	0.00	0.13	tr	0.04
Ni_2MnSb	cr				4.29	4.00		ti	0.19
Ni_2FeSb	ti	3.80	0.98	2.95	4.23	2.64	0.07	tr	0.02
Ni_2CoSb	ti	3.82	0.92	0.00	4.18	0.55	0.14	tr	0.20
Co_3In	t	3.77	0.98	4.02	4.22	4.28	0.01	t	0.40
Mn_3As	t	3.62	1.04	-1.09	4.04	2.00	0.04	t	0.33
Fe_3As	c	3.63	1.03	7.15	4.05	5.61	-0.10	t	0.47
Co_3As	t	3.60	0.97	2.60	4.06	4.35	0.27	t	0.20

'majority' and 'minority' electrons even for the case of negative m_t or m_c) will change smoothly (without flipping spin channel) when comparing compound with N_V valence electrons and similar compound with $N_V + 1$ valence electrons, or cubic and tetragonal phases. As follows from Tables I and II, such definition of the sign of the spin direction results in negative m_c for five cubic compounds: Mn_2MoGa, Mn_2MoIn, Mn_2WGa, Mn_2WIn, and Mn_3In. Four of these compounds (with exception of Mn_3In) have m_c close to $-1\mu_B$ in agreement with the Slater-Pauling rule that predicts $m_c = -1\mu_B$ for these compounds. We note also that there are 23 compounds with negative m_t in tetragonal phase and positive or zero m_c in cubic phase (see Tables I and II).

If minimal energy configuration is cubic than corresponding tetragonal configuration [tetragonal configuration with the same chemical ordering (regular or inverse) and the same initial configuration of magnetic moments as cubic configuration] may or may not exist. In the latter case only cubic lattice parameter a_c is shown in the Tables I and II and columns a_t, c'_t, m_t, and E_{ct} are empty. $E_{ct} = E_c - E_t$ is the difference between total energy of cubic configuration, E_c, and total energy of tetragonal configuration, E_t. Thus, E_{ct} is positive for tetragonal minimal energy configuration and negative for cubic minimal energy configuration.

In order to determine phase stability of the lowest energy configuration we also calculated the second minimal energy configuration, that is the configuration where the lowest local minimum of the total energy is reached in the (a, c') parameter space considering all possible magnetic and spacial (regular and inverse) configurations except the tetragonal (if exists) and cubic configurations described by the s_1 symbol and lattice parameters a_t, c'_t, and a_c. Symbol s_2 in Tables I and II describes the second minimal energy configuration using the same notations as s_1 and $E_{21} = E_2 - E_1$ is the difference between the total energy of the second lowest energy configuration, E_2, and the total energy of the lowest energy configuration, $E_1 = \min(E_t, E_c)$. In majority of cases the second minimal energy configuration has inverse(regular) structure if lowest energy configuration has regular(inverse) structure. On the other hand there are some cases when both lowest and second lowest energy configurations have the same spacial structure (regular or inverse) but different magnetic structure (e.g. ferromagnetic vs ferrimagnetic coupling of X(I) and X(II) atoms or X(I) and Y atoms). (Different magnetic structures for the same spacial structure is obtained by using different initial magnetic configurations of the atomic moments in the input of VASP calculations.) Both E_{ct} and E_{21} are shown in Tables I and II in units of eV per formula unit (4 atoms). Note that E_{21} is always positive: E_2 can be higher than both E_t and E_c, or can have a value between E_t and E_c, but cannot be lower than both E_t and E_c.

The 286 compounds that we considered in this paper is only a part of ∼2000 possible Heusler compounds. We excluded compounds with lanthanides and other heavy elements since electrodes with large concentration of heavy elements usually exhibit relatively large Gilbert damping constant due to strong spin-orbit coupling, and, according to the Slonczewski-Berger formula [20, 21], high switching current density. Also, we only considered Heusler compounds that contain at least one of three magnetic

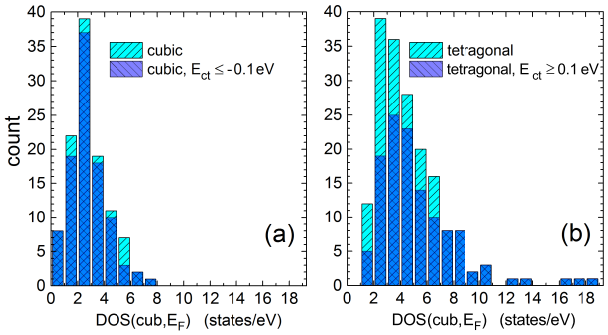

FIG. 2: Number of cubic (a) and tetragonal (b) Heusler compounds in bins corresponding to different values of $DOS(cub, E_F)$. Cyan color corresponds to 286 compounds and blue color corresponds to a subset of 220 stable compounds that have $|E_{ct}| \geq 0.1$ eV (that includes cubic compounds that do not have a metastable tetragonal phase).

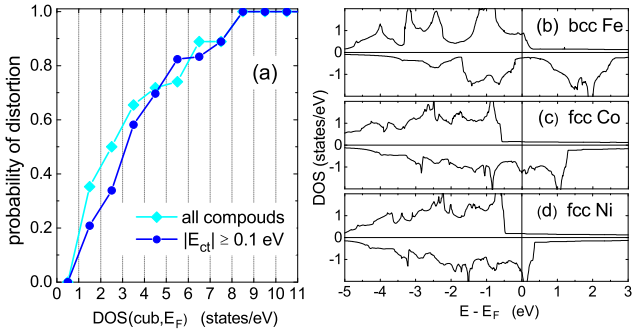

FIG. 3: (a) Probability of tetragonal distortion calculated using the data presented in Fig. 2 for corresponding $DOS(cub, E_F)$ bins, estimated from 286 compounds (cyan diamonds) and a subset of 220 stable compounds that have $|E_{ct}| \geq 0.1$ eV (blue dots). DOS of bcc Fe (b), fcc Co (c), and fcc Ni (d).

elements, Mn, Fe, or Co, since compounds with these elements (including pure Fe and Co metals) often have high Curie temperatures. High Curie temperature, $T_c >\sim 500$ K, is required for normal operation of spintronic devices. We mostly considered compounds that include late transitional metals (LTM) such as Mn, Fe, Co, Ni, Cu, Ru, Rh, Pd, Os, Ir, Pt and did not consider early transitional metals (ETM) Sc, Ti, V, Cr, Y, Zr, Nb, Hf, Ta. Note that recent calculations performed for Mn_2YGa systems [14] showed a preference of tetragonal structures for compounds with Y being the LTM rather then ETM (with an exception of Mn_2ScGa that was found to be tetragonal). We considered two elements from ETM: Y=Mo and W and, as seen from Table I, such compounds have fair share of tetragonal distortions. These results suggest that compounds with other ETMs could have fair number of tetragonally distorted cases as well. Systematic investigation of the X_2YZ Heusler compounds suitable for spintronic applications with X or Y from ETM will be the subject of another study.

IV. ORIGIN OF TETRAGONAL DISTORTION IN HEUSLER COMPOUNDS

A. Correlation of the value of $DOS(E_F)$ in cubic phase and probability of tetragonal distortion

One of our main findings is that the tetragonal distortion is common. Indeed, from 286 compounds considered, 62% are tetragonal (at zero temperature), and 43% of the 286 compounds are tetragonal with high stability with $E_{ct} \geq 0.1$eV. The percentages of tetragonal compounds for different X in X_2YZ are as follows: from 77 Mn_2YZ, 73 Fe_2YZ, 73 Co_2YZ, 18 Ni_2YZ, 15 Ru_2YZ, 15 Rh_2YZ, and 15 Pd_2YZ considered compounds, 77%, 38%, 71%, 78%, 20%, 60%, and 80%, respectively, are tetragonal.

It is generally believed that one of the main reasons for a tetragonal distortion of Heusler compounds is the DOS peaks near E_F [13, 14] in cubic phase. In order to confirm the correlation of the high value of DOS at E_F in cubic phase, $DOS(cub, E_F)$, and probability of tetragonal distortion we show the number of compounds that are stable in cubic [Fig. 2(a)] and tetragonal [Fig. 2(b)] phases in bins of $DOS(cub, E_F)$. It is seen that tetragonal compounds typically have larger $DOS(cub, E_F)$ and cubic have smaller. Cubic compounds do not have large $DOS(cub, E_F) > 8$ eV^{-1}, while 26 tetragonal compounds have $DOS(cub, E_F) > 8$ eV^{-1}. Tetragonal compounds do not have small $DOS(cub, E_F) < 1$ eV^{-1}, while 8 cubic compounds have $DOS(cub, E_F) < 1$ eV^{-1}.

In Fig. 3(a) the probability of finding a tetragonal distortion is shown versus $DOS(cub, E_F)$ bins by cyan line. The probability is defined as the number of tetragonal compounds [from Fig. 2 (b)] within a corresponding $DOS(cub, E_F)$ bin divided by the number of all compounds [from Figs. 2(a),(b)] in this bin. The probability of finding a distortion is zero for $DOS(cub, E_F) < 1$ eV^{-1} and monotonically increases with increasing $DOS(cub, E_F)$. The probability passes 50% at $DOS(cub, E_F) \sim 2.5$ eV^{-1} and reaches 100% at $DOS(cub, E_F) \gtrsim 8$ eV^{-1}. Blue line in Fig. 3(a) shows the probability of a distortion when only stable compounds with $|E_{ct}| \geq 0.1$eV are considered (including cubic compounds that do not have a tetragonal phase). The probability significantly reduces in the region of small $DOS(cub, E_F) < 3$ eV^{-1} since the number of stable tetragonal Heuslers with $E_{ct} \geq 0.1$eV significantly reduces for small $DOS(cub, E_F)$, see Fig 2(b). Fig. 3(a) shows the strong correlation between the value of $DOS(cub, E_F)$ and the probability of finding a tetragonal distortion and, in particular, that it is highly unlikely for cubic compounds *not* to undergo a distortion if $DOS(cub, E_F) \gtrsim 7$ eV^{-1}.

Fig 4 shows the DOS in the tetragonal phase at E_F, $DOS(tet, E_F)$, as a function of $DOS(cub, E_F)$ for 191 compounds that have a tetragonal phase. One can see that there are only three stable cubic compounds with

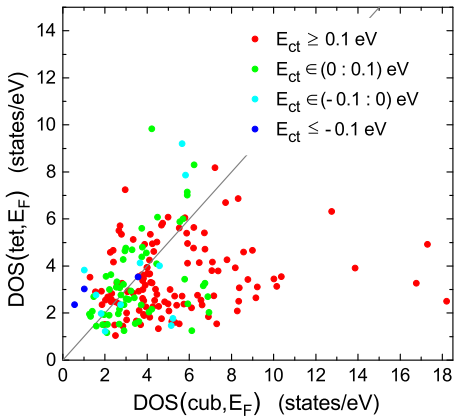

FIG. 4: $DOS(tet, E_F)$ as a function of $DOS(cub, E_F)$ for 191 Heusler compounds that have a tetragonal phase (see text for details).

$E_{ct} < -0.1$ eV. For all three compounds $DOS(tet, E_F) > DOS(cub, E_F)$, as expected.

One can see in Fig 4 that the majority of stable tetragonal compounds with $E_{ct} > 0.1$ eV have $DOS(tet, E_F) < DOS(cub, E_F)$ and those that do not satisfy this inequality either have $DOS(tet, E_F)$ just above the $DOS(tet, E_F) = DOS(cub, E_F)$ line or have small $DOS(cub, E_F) < 3$ eV^{-1}, or both. Only three stable tetragonal compounds with $DOS(cub, E_F) > 5$ eV^{-1} have $DOS(tet, E_F) > DOS(cub, E_F)$ and all three have $DOS(tet, E_F)$ rather close to the line $DOS(tet, E_F) = DOS(cub, E_F)$. Thus, we conclude that large $DOS(cub, E_F)$ is indeed one of the main reasons for a tetragonal distortion, and that after the tetragonal distortion $DOS(E_F)$ is typically reduced.

B. Probability of high $DOS(E_F)$ in cubic phase and reasons for lowering $DOS(E_F)$ in tetragonal phase

As one can see in the Supplemental Material [22], the DOS of cubic phases of Heusler compounds have, in general, a pronounced peak-and-valley character. The peak-and-valley character of the DOS of Heusler compounds is a consequence of the highly localized d-bands (see Ref. [23] for general description of bands in cubic Heuslers) and the van Hove singularities at the band edges of these d-bands. From the analysis of the 286 compounds we conclude that the main reason why *so many* Heusler compounds have a tetragonal distortion is the peak-and-valley character of the DOS in the cubic phases in conjunction with a "smooth shift" of the majority or/and minority DOS relative to E_F when valence electrons are added to the system. (By "smooth shift" we mean a shift of the DOS structure that preserves the order of the peaks and valleys, at least near E_F.)

Let us consider a cubic compound that has a peak-and-valley DOS with typical DOS values, DOS_p, in the pick regions and typical DOS values, DOS_v, in the valley regions ($DOS_p \gg DOS_v$). If we shift DOS relative to E_F with a condition to fill some random number of states then probability for E_F to end up in the peak region is $DOS_p/DOS_v \gg 1$ higher than probability for E_F to end up in the valley region (we assume here that the energy widths of the peak and valley regions are comparable). Such simple probabilistic consideration explains why many cubic compounds have E_F in the middle of the DOS peak. In magnetic systems having E_F at energetically unfavourable position near DOS peaks can be avoided since DOS structures can be shifted independently in two spin channels. On the other hand, if DOS in one of the spin channel does not shift relative to E_F for some reasons (e.g. due to energetically favorable position of E_F inside the DOS valley in this spin channel, as we demonstrate below on an example of Mn_2YGa series) addition of electrons to the system forces shift of the DOS structure in another spin channel that often results in having E_F at the DOS peak in this spin channel.

When E_F is in the middle of a DOS peak the $DOS(E_F)$ could be lowered by a tetragonal distortion [24] for several possible reasons, as follows. Firstly, a cubic system has many points, lines, and surfaces in the Brillouin zone that are equivalent by symmetry. The energies of the bands at equivalent k-points are the same. After tetragonal distortion some of these k-points become inequivalent resulting in unequal energy values at these points and, therefore, in less peaky structure of the DOS. Secondly, when there is a degeneracy of occupied states at a high-symmetry k-point (such as the Γ-point) with energy near E_F, the degeneracy can be lifted by lowering the symmetry of the system, so some states shift to lower energies while another states become unoccupied (a band Jahn-Teller effect) [5, 13]. Thirdly, the bands, that are derived from orbitals which overlap along the direction of the crystal contraction, become broader following a distortion [25]. All three effects result in a reduction (and/or shift away from E_F) of the DOS peaks and, in general, a more smoothly distributed DOS in a tetragonal phase as compared to cubic phase. In addition, the tetragonal phase has two independent lattice parameters instead of just one in a cubic phase. This additional degree of freedom also helps to avoid DOS peaks at E_F.

Since one of the contributions to the total energy is the band energy $E_{band} = \int_{E_{min}}^{E_F} dEDOS(E)E$, a reduction of the DOS near E_F in a tetragonal phase, in conjunction with conservation of the integral for the number of valence electrons $N_V = \int_{E_{min}}^{E_F} dEDOS(E)$ often leads to a lower band energy and, thus, to a lower total energy of the tetragonal phase as compared to the cubic phase. [E_{min} here is the minimum energy of the valence bands.] We note although that while the mechanism of the tetragonal distortion due to the DOS peaks at E_F describes the distortion in majority of Heusler compounds, in some cases the energy stability of the cubic phase could not be simply derived from presence or absence of the DOS peaks near E_F. One reason for this is that the total energy is a complex entity that has other contributions beyond sim-

ple band energy contribution that could be important in determining the lowest energy phase.

C. Tetragonal distortion in compounds of Mn_2YGa series with Y=Mn,Fe,Co,Ni,Cu

We illustrate the concept of the smooth DOS shifts that induce alternating stable and non-stable cubic configurations on an exemplary system Mn_2YGa, by considering addition of the valence elections, one by one, to the system, by varying Y. Fig. 5 shows the DOS of cubic phase and corresponding tetragonal phase for the inverse Mn_2YGa with Y=Mn,Fe,Co,Ni,Cu. As seen in Fig 5(a) the cubic Mn_3Ga has a peak at E_F in the majority DOS and the so-called SP valley [23] in minority DOS that is responsible for predicted Slater-Pauling behaviour of magnetic moments in many cubic Heusler compounds. The peak in the majority DOS just below E_F originates from the van Hove singularity associated with doubly-degenerate e_g bands at the Γ-point [13]. The tetragonal distortion of Mn_3Ga leads to a splitting of these bands to $d_{x^2-y^2}$ and d_{z^2} bands with distinct energies of $E_F + 0.2$ eV and $E_F - 0.7$ eV at the Γ-point. Thus, the tetragonal distortion lowers the $DOS(E_F)$ [see Fig. 5(f)] and thereby lowers the total energy ($E_{ct} = 0.19$eV).

As N_V is increased by 1 from Mn_3Ga to Mn_2FeGa [Fig 5 (b)], the SP valley in minority DOS does not shift relative to E_F (in general, E_F is 'sticky' with respect to the SP valley [23], since the position of E_F within the valley is energetically-favorable), while the majority DOS shifts to lower energies. The DOS peak that was at $E_F + 0.5$ eV in Mn_3Ga is now exactly at E_F in Mn_2FeGa. The position of E_F in the middle of the peak can be explained as follows. First, since E_F stays within the SP valley in minority DOS there are no two degrees of freedom anymore, namely, independent shift of minority and majority bands. Second, when there is only one degree of freedom (shift of majority DOS), than, as discussed above, the probability of E_F ending up after the shift within a DOS peak region is higher than within a valley region. Thus, even if it is energetically-unfavorable, the position of E_F in the middle of the peak is forced by the need to accommodate an additional electron.

Due to the peak in DOS at E_F the cubic phase of Mn_2FeGa is unstable. The tetragonal distortion lowers the $DOS(E_F)$ [see Fig. 5(g)] and the total energy ($E_{ct} = 0.14$ eV). The DOS peak at E_F in Mn_2FeGa originates mostly from a van Hove singularity of a single flat band localized on Fe atom, which, as was noted in [14], is a deviation from other models, where the tetragonal distortion in Mn_2YZ Heuslers is thought to originate from *d*-bands localized at octahedrally coordinated Mn atoms.

Going from Mn_2FeGa to Mn_2CoGa [Fig 5 (c)], the SP valley in the minority DOS is still intact, while the valley in the majority DOS that was at $E_F + 0.4$ eV in Mn_2FeGa is now exactly at E_F. Because of the double valley at E_F in both the minority and majority DOS the cubic phase of Mn_2CoGa is more stable than the tetragonal phase.

Going from Mn_2CoGa to Mn_2NiGa [Fig 5 (d)], now the valley in the majority DOS holds, while the SP valley in the minority DOS finally shifts to lower energies. This shift results in a (modest) peak in the minority DOS at E_F which is smoothed out after a distortion. The DOS of the tetragonal phase has a double valley at E_F [see Fig. 5(i)] leading to lower total energy ($E_{ct} = 0.12$ eV).

Going from Mn_2NiGa to Mn_2CuGa [Fig 5 (e)], the valley in the majority DOS still holds, while the valley in the minority DOS shifts to even lower energies with more or less a smooth distribution of the minority states in the energy window ($E_F - 1.5$ eV, $E_F + 0.7$ eV) that results in a relatively small value of $DOS(cub, E_F)$ and, thus, a stable cubic compound without a tetragonal phase.

In considered Mn_2YGa Y-series and most of the other Y- and Z-series (see Supplemental material) the Fermi energy works as a sensor of the peak-and-valley DOS structure with corresponding alternations of stable [low $DOS(cub, E_F)$] and non-stable [high $DOS(cub, E_F)$] cubic phases when the DOS shifts relative to E_F. Similar DOS shift when (a fraction of) a valence electron is added to a system (using suitable substitutions) was also proposed in the design scheme of PMA Heusler compounds [13] in order to force the tetragonal distortion.

D. Probability of tetragonal distortion for different classes of Heusler compounds

Mn_2YZ compounds are very susceptible to a tetragonal distortion (77% of considered Mn_2YZ compounds are tetragonal) due to a peaky structure of the *majority* DOS in the vicinity of E_F and a smooth shift of this DOS structure to lower energies within the Y-series. Fe_2YZ and Ru_2YZ compounds have a small share of tetragonal compounds (38% and 20%). One reason for this is that for compounds with X=Fe,Co,Ni,Ru,Rh,Pd the peaks at E_F in majority DOS are rare (except when Y=Mn, see Supplemental Material) due to preferred ferromagnetic coupling of two X atoms and shift of most of the DOS peaks in majority spin channel below E_F. Secondly, the parent material - bcc Fe - has a broad valley in the minority DOS near E_F [see Figs. 3 (b)]. Thirdly, the SP valley in minority DOS (with E_F within this valley) more frequently occur for Heuslers with X=Mn,Fe as compared to heavier X=Co,Ni [23]. As a result, the peaks in both minority and majority DOS for many compounds with X=Fe,Ru are rarely located near E_F that explains large number of stable cubic phases in these compounds. Tetragonal distortions mostly occur for small subset of heavier Fe_2YZ (Y=Cu,Pd,Pt) and Ru_2CoZ, in which the SP valley is moved below E_F or closed.

A large proportion of Co_2YZ and Ni_2YZ compounds are tetragonal (71% and 78%) due to the elevated *minority* DOS values near E_F in the parent materials - fcc Co and fcc Ni metals [see Figs. 3 (c),(d)] that leads to a peaky *minority* DOS structure near E_F in Co_2YZ and

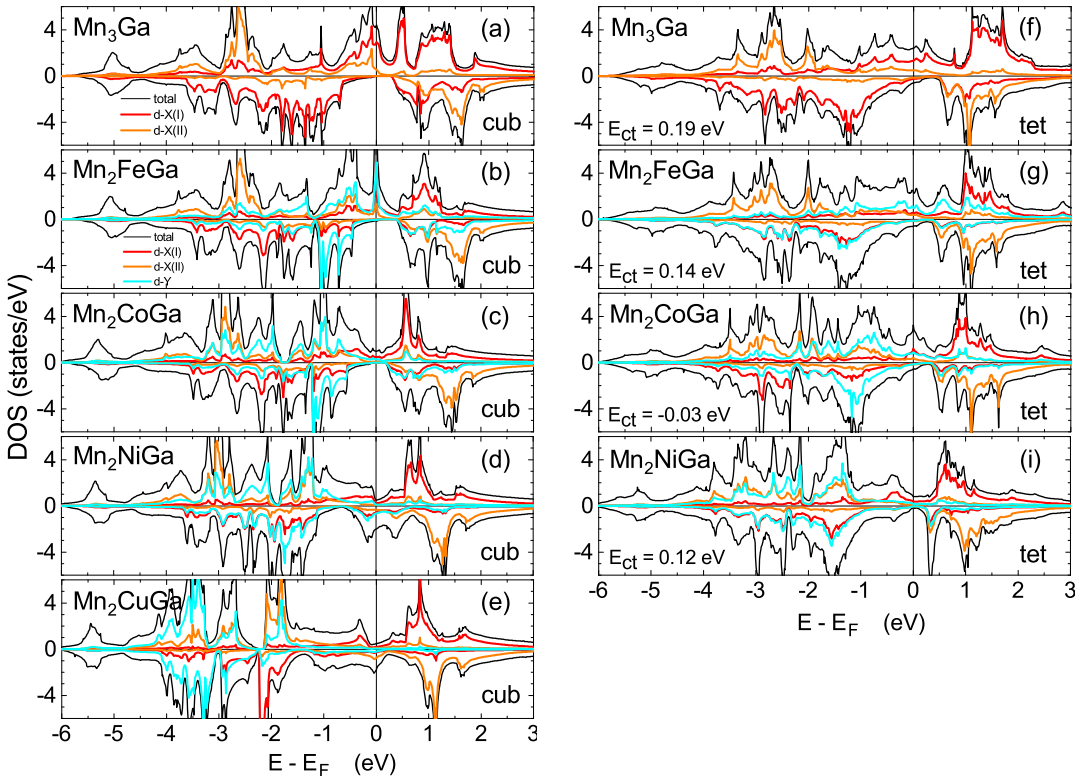

FIG. 5: DOS for majority ($DOS > 0$) and minority ($DOS < 0$) electron bands of cubic (marked as 'cub', left panels) and tetragonal (marked as 'tet', right panels) inverse Mn_2YGa compounds with Y=Mn,Fe,Co,Ni, and Cu. E_{ct} values are shown in the figures in the right (tetragonal) panels. The black curves show the total DOS for each electron spin. Red, orange, and cyan curves show the partial DOS projected into the d-orbitals of tetrahedrally coordinated (by Ga) Mn, octahedrally coordinated (by Ga) Mn, and Y atoms, respectively.

Ni_2YZ. Small fraction of Co_2YZ compounds that are cubic mostly have lighter Y=Mn,Fe with the SP valley in minority DOS that stabilizes the cubic phase. Since Rh and Pd have the same valence as Co and Ni, respectively, the compounds with X=Rh,Pd have similar DOS structures as those with X=Co,Ni and, thus, similarly a large share of tetragonal distortions (60% and 80%).

We found that 97% of considered ternary compounds with the same X and Y, and Z from the same group (Z=Al,Ga,In or Z=Si,Ge,Sn), and 93% ternary compounds with the same X and Z, and Y from the same group (Y=Fe,Ru,Os, or Y=Co,Rh,Ir, or Y=Ni,Pd,Pt, or Y=Mo,W), have the same regular or inverse minimum energy configuration. Morover, 85% of considered compounds with the same X and Y, and Z from the same group, and 90% of compounds with the same X and Z, and Y from the same group, have the same tetragonal or cubic minimum energy configuration. Thus, Y (and Z) elements from the same group have similar effect on defining the stable configuration (regular vs inverse and tetragonal vs cubic) in majority of Heusler compounds.

V. CHEMICAL ORDERING AND MAGNETIC STRUCTURE OF TETRAGONAL HEUSLER COMPOUNDS

The rules that governs the chemical ordering of cubic Heusler compounds are derived in Ref [23]. In particular, 128 out of 132 (97%) considered in Ref [23] cubic compounds X_2YZ with X=Mn or Fe satisfy the so-called 'lightest atom' rule for the chemical ordering that states that the cubic Heusler compound X_2YZ is stable in whichever phase (regular or inverse) in which site II is occupied by the 'lightest atom' - the lower-valence atom or atom with smaller atomic number if the valence of X and Y atoms is the same. The 'lightest atom' rule also works rather well for cubic compounds with X=Co,Ni,Ru,Rh,Pd for low-valence Y atoms such as W or Mo, but it is often violated for higher-valence Y atoms such as Fe, Co or Ni.

General trends in magnetic structure of cubic Heusler compounds are also described in [23]. In particular, it has been shown that majority of cubic compounds with X=Mn and Y atoms with valence higher than Mn (Y=Fe,Co,Ni, etc) have inverse structure with antiferromagnetic (AFM) coupling of two X atoms, while compounds with X=Mn and Y atoms with valence lower than Mn (Y=Mo or W) have ether regular non-magnetic

structure or regular structure with FM coupling of two Mn atoms. Vast majority of cubic compounds with X=Fe,Co,Ni have ferromagnetic (FM) coupling of X atoms.

Tables I and II show that majority (72%) of 286 considered in present paper Heusler compounds ether have cubic lowest energy configuration or tetragonal lowest energy configuration with energy of corresponding cubic phase lower than the energy of any other configuration with competing atomic and/or magnetic order ($E_{ct} < E_{21}$ in Tables I and II). In particular, the subset of such compounds includes 56 out of 77 (73%), 56 out of 73 (77%), 43 out of 73 (59%), 13 out of 18 (73%), 12 out of 15 (80%), 14 out of 15 (93%), and 13 out of 15 (87%) of considered compounds with X=Mn,Fe,Co,Ni,Ru,Rh, and Pd, correspondingly. Since we define the cubic phase that corresponds to the tetragonal lowest energy configuration as one that has the same as the tetragonal phase chemical order (regular or inverse) and the same initial configuration of magnetic moments in the input of the VASP program, the 'lightest atom rule' for chemical order is valid (invalid) for the tetragonal phase of compounds from the above subset if it is valid (invalid) for corresponding cubic phase. For the same reason magnetic coupling of two X atoms (AFM or FM) was found to be the same for majority of tetragonal and corresponding cubic phases for above subset of compounds. Therefore, the chemical (regular or inverse) and magnetic (AFM or FM) structure of the tetragonal phase for above subset of compounds is described by the same rules [23] that governs the cubic phase.

For remaining (minority of) compounds with tetragonal lowest energy configuration and $E_{ct} > E_{21}$ (which means that some competing, tetragonal or cubic, configuration, s_2, exists with energy E_2 lower than the energy of corresponding cubic phase, E_c) the chemical ordering (in most cases) and/or magnetic structure in the lowest-energy tetragonal phase often differs from that in the lowest-energy cubic phase. While for most of tetragonal compounds with X=Fe,Co,Ni and $E_{ct} > E_{21}$ two X atoms are still FM coupled in tetragonal phase, the magnetic structure of substantial share of tetragonal compounds with X=Mn and $E_{ct} > E_{21}$ changes from the AFM coupling in cubic phase to the FM coupling in tetragonal phase. For example, for compounds Mn_2CuSi, Mn_2CuGe, Mn_2CuSn, Mn_2CuSb, Mn_2NiSb, and Mn_2PdSb the atomic and magnetic configuration changes from inverse AFM configuration in cubic phase to regular FM configuration in tetragonal phase.

We found that majority of tetragonal compounds with X=Fe and $E_{ct} > E_{21}$ have chemical ordering in disagreement with the 'lightest atom rule', while cubic phases of these compounds almost always satisfy the 'lightest atom rule'. On the other hand, majority of tetragonal compounds with X=Co and $E_{ct} > E_{21}$ have chemical ordering in agreement with the 'lightest atom rule' (in many cases cubic phase of such compounds also satisfy the 'lightest atom rule'). The reason for the change of the chemical ordering in the lowest-energy tetragonal phase for compounds with $E_{ct} > E_{21}$ as compared to the chemical ordering in the lowest-energy cubic phase is still not well understood and needs further investigation.

VI. ACCURACY OF CALCULATIONS AND EFFECT OF THE SPIN-ORBITAL COUPLING

We verified that presented in Tables I and II results are converged by varying the number of divisions in reciprocal space from 10×10×10 to 18×18×18 and the energy cutoff from 400 eV to 520 eV. Presented in Tables I and II results are obtained without considering the spin-orbital coupling (SOC). We verified that inclusion of the SOC has negligible effect on the lattice constants (the change is less than 0.005 Å). The effect of the SOC on the E_{ct} is more noticeable. We calculated the effect of the SOC on E_{ct} for subset of 123 stable tetragonal compounds that have both $E_{ct} \geq 0.05$ eV and $E_{21} \geq 0.05$ eV. Table III shows the E_{ct} calculated without taking into account the SOC, the E_{ct}^{so} calculated with taking into account the SOC, and the difference $\Delta_{ct}^{so} = E_{ct}^{so} - E_{ct}$ for 13 (out of 123 considered) compounds that have $|\Delta_{ct}^{so}| \geq 0.01$ eV. As expected, the SOC is significant mainly for heavy compounds - 12 out of 13 compounds with $|\Delta_{ct}^{so}| \geq 0.01$ eV have Y=Os,Ir, or Pt. As one can see in Table III, the sign of the E_{ct}^{so} and E_{ct} is the same in all considered cases, therefore the SOC does not affect any conclusions derived above regarding stability of different phases of Heusler compounds .

In Table IV we compare results obtained in present work by using the PAW approach as implemented in VASP program with PBE GGA/DFT functionals and results obtained in Ref. [6, 14] by using the all-electron FP-LAPW approach as implemented in WIEN2k program with PBE GGA/DFT functionals. The chemical ordering (inverse or regular, marked as 'inv' or 'reg') of presented compounds corresponds to the ordering of the lowest-energy cubic phase. The lowest-energy tetragonal phase (when exists) has the same chemical ordering as the lowest-energy cubic phase for all compounds in Table IV except Mn_2PtSn, for which lowest-energy cubic phase is inverse, while lowest-energy tetragonal phase is regular (see Table I). [Results are presented for inverse cubic and inverse tetragonal structures for Mn_2PtSn in Table IV.] As one can see, the PAW and FP-LAPW results, in general, have excellent agreement between each other except three discrepancies discussed below.

First, our lattice constants for tetragonal phase of Mn_3Ga, $a = 3.78$Å and $c' = 0.94$, differ from $a = 3.90$Å and $c' = 0.91$ obtained in Ref [14]. On the other hand, our lattice constants for Mn_3Ga are in excellent agreements with lattice constants $a = 3.77$Å and $c' = 0.95$ obtained in Ref [6] where the same WIEN2k code has been used as in Ref. [14]. The discrepancy between results of works [14] and [6] for Mn_3Ga could be due to the entry error in Ref [14] (there is an obvious entry error in Ref. [14] in the table line that corresponds to Mn_3Ga - cited ex-

TABLE III: E_{ct} calculated without taking into account the SOC, the E_{ct}^{so} calculated with taking into account the SOC, and the difference $\Delta_{ct}^{so} = E_{ct}^{so} - E_{ct}$ for 13 (out of 123 considered) Heusler compounds that have $|\Delta_{ct}^{so}| \geq 0.01$ eV.

	E_{ct} (eV)	E_{ct}^{so} (eV)	Δ_{ct}^{so} (eV)		E_{ct} (eV)	E_{ct}^{so} (eV)	Δ_{ct}^{so} (eV)		E_{ct} (eV)	E_{ct}^{so} (eV)	Δ_{ct}^{so} (eV)
Mn_2OsGa	0.15	0.17	0.02	Fe_2PtGe	0.60	0.57	-0.03	Co_2IrIn	0.18	0.20	0.02
Mn_2OsGe	0.06	0.08	0.02	Fe_2PtSb	0.40	0.37	-0.03	Co_2PtGe	0.52	0.50	-0.02
Mn_2OsSn	0.33	0.34	0.01	Co_2OsGa	0.25	0.21	-0.04	Co_2PtSn	0.49	0.48	-0.01
Mn_2OsSb	0.24	0.26	0.02	Co_2IrGa	0.05	0.07	0.02	Co_2OsSb	0.23	0.24	0.01
								Rh_2FeSb	0.37	0.36	-0.01

TABLE IV: Comparison of results obtained in present work by using the PAW approach as implemented in VASP program with PBE GGA/DFT functionals and results obtained in Ref. [6, 14] by using the all-electron FP-LAPW approach as implemented in WIEN2k program with PBE GGA/DFT functionals. The chemical ordering (inverse or regular, marked as 'inv' or 'reg') of presented compounds corresponds to the ordering of the lowest-energy cubic phase.

		a_t (Å)	c_t'	m_t (μ_B)	a_c (Å)	m_c (μ_B)	E_{ct} (eV)	Ref			a_t (Å)	c_t'	m_t (μ_B)	a_c (Å)	m_c (μ_B)	E_{ct} (eV)	Ref
Mn_2FeGa	inv	3.69	0.98	-0.84	4.09	1.02	0.14		Mn_2IrGa	inv	3.83	0.97	0.07	4.21	2.00	0.27	
	inv	3.68	0.99	-0.78	4.09	1.03	0.14	[14]		inv	3.83	0.97	0.11	4.22	2.00	0.27	[14]
Mn_2CoGa	inv	3.71	0.96	0.14	4.08	2.00	-0.03		Mn_2PtGa	inv	3.90	0.94	0.87	4.33	0.47	0.18	
	inv	3.71	0.96	0.17	4.09	2.00	-0.03	[14]		inv	3.91	0.93	0.75	4.33	0.44	0.17	[14]
Mn_2NiGa	inv	3.79	0.90	0.99	4.13	1.16	0.12		Mn_2OsSn	inv	3.96	0.98	-0.02	4.37	2.00	0.33	
	inv	3.79	0.91	1.00	4.14	1.18	0.15	[14]		inv	3.97	0.98	-0.02	4.39	1.50	0.21	[14]
Mn_2CuGa	inv				4.20	0.30			Mn_2IrSn	inv	3.99	0.96	0.46	4.45	0.44	0.22	
	inv				4.20	0.33		[14]		inv	4.01	0.96	0.45	4.46	0.41	0.10	[14]
Mn_2MoGa	reg				4.17	-1.00			Mn_2PtSn	inv	4.14	0.91	-0.02	4.52	0.17	0.11	
	reg				4.18	-1.01		[14]		inv	4.15	0.91	-0.02	4.52	0.19		[14]
Mn_2RuGa	inv	3.81	0.97	-0.26	4.21	1.02	0.10		Mn_2OsIn	inv	3.92	1.01	-0.29	4.42	0.68	0.36	
	inv	3.80	0.98	-0.24	4.22	1.03	0.12	[14]		inv	3.93	1.01	-0.27	4.43	0.62	0.40	[14]
Mn_2RhGa	inv	3.83	0.97	0.07	4.23	1.68	0.17		Mn_2IrIn	inv	3.96	0.99	0.04	4.45	0.71	0.31	
	inv	3.82	0.97	0.10	4.23	1.64	0.18	[14]		inv	3.97	0.99	0.07	4.45	0.68	0.35	[14]
Mn_2PdGa	inv	3.93	0.92	0.92	4.33	0.55	0.10		Mn_2PtIn	inv	4.11	0.92	0.44	4.51	0.32	0.08	
	inv	3.93	0.92	0.93	4.33	0.55	0.10	[14]		inv	4.12	0.92	0.38	4.51	0.31	0.08	[14]
Mn_2WGa	reg				4.18	-0.95			Mn_2FeGe	inv	3.62	1.03	-0.86	4.05	2.00	-0.06	
	reg				4.19	-0.94		[14]		inv	3.63	1.02	-0.06	4.05	2.01	-0.07	[14]
Mn_2OsGa	inv	3.80	0.98	-0.28	4.21	1.00	0.15		Mn_3Ge		3.73	0.95	-1.01	4.06	1.00	0.10	
	inv	3.80	0.98	-0.28	4.21	1.02	0.14	[14]			3.74	0.95	-0.98	4.07	1.01	0.06	[14]
									Mn_3Ga		3.78	0.94	-1.79	4.12	0.00	0.19	
											3.90	0.91	-1.89	4.12	0.01	0.15	[14]
											3.77	0.95	-1.77				[6]

perimental value of $c/a = 1.77$ does not agree with cited in the same line experimental values of $a = 3.77$Å and $c = 7.16$Å).

Two other minor discrepancies between our results and results obtained in Ref. [14] are in the values of the magnetic moment of cubic phase of Mn_2OsSn (difference is 0.5 μ_B) and magnetic moment of tetragonal phase of Mn_2FeGe (difference is 0.8 μ_B). We note that our value of $2.00\mu_B$ for magnetic moment of cubic Mn_2OsSn agrees with that predicted by the Slater-Pauling rule (see the SP valley at E_F in the minority DOS of Mn_2OsSn in Supplemental Material).

VII. CONCLUSION

In existing literature researchers usually explain the tetragonal distortion of individual Heusler compounds by studying the origin of particular DOS peaks near E_F. In present paper we followed somewhat different approach and tried to find some general reasons for tetragonal distortion of broad classes of Heusler compounds and explain why in some of these classes distortion occurs very often and in other classes it it relatively rare. We found that the tetragonal distortion is very common in Heusler compounds. From 286 compounds that we examined 62% are tetragonal and 43% are tetragonal with considerable stability ($E_{ct} \geq 0.1$ eV). A large share of these tetragonal compounds can be accounted for by the general character of the peak-and-valley structure of the DOS of cubic Heusler compounds (arising from localized d-bands and van Hove singularities) in conjunction with a smooth shift of this peaky DOS structure relative to E_F when valence electrons are added to the system. A shift of DOS in X_2YZ compounds within Y-series (or Z-series) leads to an alternation between stable and unstable cubic phases depending on the value of $DOS(cub, E_F)$. The probability of a tetragonal distortion strongly correlates with $DOS(cub, E_F)$ - the probability increases when $DOS(cub, E_F)$ increases [see Fig. 3 (a)]. We identified the sub-groups of compounds with large (X=Mn,Co,Ni,Rh,Pt) and small (X=Fe,Ru) share

of tetragonal distortions and explained this behaviour. Finally, we found that Y (and Z) elements from the same group have a similar effect on determining the stable phase in majority of Heusler compounds.

We believe that the understanding of the mechanism of tetragonal distortion in Heusler compounds described in this paper will be instrumental for both experimental and theoretical efforts in finding tetragonal Heuslers with high PMA from among more than 2000 members of Heusler family. Finding of such materials is of significant technological interest in the context of novel spintronic applications such as STT-MRAM technology.

Acknowledgement

S.F. acknowledges the CNMS User support by Oak Ridge National Laboratory Division of Scientific User facilities. S.F. thanks Oleg Mryasov for useful discussions and Elena Faleeva for preparing the picture of Heusler structure.

[1] S. Ikeda, K. Miura, H. Yamamoto, K. Mizunuma, H. D. Gan, M. Endo, S. Kanai, J. Hayakawa, F. Matsukura, and H. Ohno,*A perpendicular-anisotropy CoFeB-MgO magnetic tunnel junction.* Nat. Mater. **9**, 721 (2010).

[2] H. Sato, E. C. I. Enobio, M. Yamanouchi, S. Ikeda, S. Fukami, S. Kanai, F. Matsukura, and H. Ohno, *Properties of magnetic tunnel junctions with a MgO/CoFeB/Ta/CoFeB/MgO recording structure down to junction diameter of 11 nm.* Appl. Phys. Lett. **105**, 062403 (2014).

[3] S. S. P. Parkin, *MgO Tunnel barriers and method of formation.* US patent 8,008,097 (2003).

[4] Stuart. S. P. Parkin, Christian Kaiser, Alex Panchula, Philip M. Rice, Brian Hughes, Mahesh Samant, and See-Hun Yang, *Giant tunneling magnetoresistance at room temperature with MgO (100) tunnel barriers.* Nat. Mater. **3**, 862 (2004).

[5] T. Graf, C. Felser, and S. S. P. Parkin, *Simple rules for the understanding of Heusler compounds.* Prog. Solid State Chem. **39**, 1 (2011).

[6] B. Balke, G. H. Fecher, J. Winterlik, and C. Felser, *Mn_3Ga, a compensated ferrimagnet with high Curie temperature and low magnetic moment for spin torque transfer applications.* Appl. Phys. Lett. **90**, 152504 (2007).

[7] H. Kurt, N. Baadji, K. Rode, M. Venkatesan, P. Stamenov, S. Sanvito, and J. M. D. Coey, *Magnetic and electronic properties of $D0_{22}$-Mn_3Ge (001) films.* Appl. Phys. Lett. **101**, 132410 (2012).

[8] A. Sugihara, S. Mizukami, Y. Yamada, K. Koike, and T. Miyazaki, *High perpendicular magnetic anisotropy in $D0_{22}$-$Mn_{3+x}Ge$ tetragonal Heusler alloy films.* Appl. Phys. Lett. **104**, 132404 (2014).

[9] S. Mizukami, A. Sakuma, A. Sugihara, T. Kubota, Y. Kondo, H. Tsuchiura and T. Miyazaki, *Tetragonal $D0_{22}$ $Mn_{3+x}Ge$ Epitaxial Films Grown on MgO(100) with a Large Perpendicular Magnetic Anisotropy.* Appl. Phys. Expr **6**, 123002 (2013).

[10] M. Li, X. Jiang, M. G. Samant, C. Felser, and S. S. P. Parkin, *Strong dependence of the tetragonal $Mn_{2.1}Ga$ thin film crystallization temperature window on seed layer.* Appl. Phys. Lett. **103**, 032410 (2013).

[11] A. Köhler, I. Knez, D. Ebke, C. Felser, and S. S. P. Parkin, *Loss of anisotropy in strained ultrathin epitaxial L10 Mn-Ga films.* Appl. Phys. Lett. **103**, 162406 (2013).

[12] J. Jeong, Y. Ferrante, S. V. Faleev, M. G. Samant, C. Felser, and S. S. P. Parkin, *Termination layer compensated tunnelling magnetoresistance in ferrimagnetic Heusler compounds with high perpendicular magnetic anisotropy.* Nat. Commun. **6**, 10276 (2015).

[13] J. Winterlik, S. Chadov, A. Gupta, V. Alijani, T. Gasi, K. Filsinger, B. Balke, G. H. Fecher, C. A. Jenkins, F. Casper, J. Kbler, G.-D. Liu, L. Gao, S. S. P. Parkin, C. Felser, *Design scheme of new tetragonal Heusler compounds for spin-transfer torque applications and its experimental realization.* Adv. Mater. 24, 6283 (2012)

[14] L. Wollmann, S. Chadov, J. Kübler, and C. Felser, *Magnetism in tetragonal manganese-rich Heusler compounds.* Phys. Rev. B **92**, 064417 (2015)

[15] G. Kresse and J. Furthmuller, *Efficient iterative schemes for ab initio total-energy calculations using a plane-wave basis set.* Phys. Rev. B **54**, 11169 (1996).

[16] P. E. Blöchl, *Projector augmented-wave method.* Phys. Rev. B **50** 17953 (1994).

[17] G. Kresse and D. Joubert, *From ultrasoft pseudopotentials to the projector augmented-wave method.* Phys. Rev. B **59**, 1758 (1999).

[18] J. Kübler, *First principle theory of metallic magnetism.* Physica B+C **127**, 257 (1984).

[19] I. Galanakis, P. H. Dederichs, and N. Papanikolaou, *Slater-Pauling behavior and origin of the half-metallicity of the full-Heusler alloys.* Phys. Rev. B **66**, 174429 (2002).

[20] J. Slonczewski, *Current-driven excitation of magnetic multilayers.* J. Magn. Magn. Mater. **159**, L1 (1996).

[21] L. Berger, *Emission of spin waves by a magnetic multilayer traversed by a current.* Phys. Rev. B **54**, 9353 (1996).

[22] See Supplemental Material at [URL inserted by publisher] for DOS figures of cubic and tetragonal (when exists) phases of 286 considered Heusler compounds.

[23] S. V. Faleev, Y. Ferrante, J. Jeong, M. G. Samant, B. Jones, and S. S. P. Parkin, *Unified explanation of chemical ordering, the Slater-Pauling rule, and half-metallicity in full Heusler compounds*, Phys. Rev. B (2017). [accepted, APS idintification LS15438B]

[24] While other distortion types such as orthorhombic or rhombohedral are also possible, in this paper we only consider tetragonal distortion type. In MTJ devices square structure in the xy-plane is often preferred due to the square translation symmetry of the underlayer and/or overlayer materials.

[25] J. C. Suits, *Structural instability in new magnetic Heusler compounds.* Solid State Comm. **18**, 423 (1976).